DETECTION OF TURBULENT COHERENT MOTIONS IN A FOREST CANOPY
PART II: TIME-SCALES AND CONDITIONAL AVERAGES

SERGE COLLINEAU

Station de Bioclimatologie-INRA, 78850 Thiverval-Grignon, France

and

YVES BRUNET

Station de Bioclimatologie-INRA, BP 81, 33883 Villenave d'Ornon, France

(Received in final form 4 January, 1993)

Abstract. Turbulent exchanges between plant canopies and the atmosphere are known to be strongly affected by intermittent coherent motions, which appear on time traces of turbulent variables as periodic, large-amplitude excursions from the mean. Detecting these features requires objective and powerful signal analysis techniques. We investigate here the possibilities offered by the recently developed *wavelet transform*, presented in a companion paper. For this purpose, a set of data acquired in a 13.5 m high pine forest in southwestern France was used, which provided time series of wind velocities and air temperature recorded at two levels simultaneously, under moderately unstable conditions. Firstly, a duration scale of the active part of coherent motions was estimated from the wavelet variance. Then, we focused on the detection itself of large-scale features; several wavelet functions were tested, and the results compared with those obtained from more classical conditional sampling methods such as VITA and WAG. A mean time interval $\Delta = 1.8h/u_*$ (h being the canopy height and u_* the friction velocity) between contiguous coherent motions was obtained. The features extracted from the various traces and ensemble-averaged over 30 min periods appeared very similar throughout the four hours of data studied. They provided a dynamic description of the ejection-sweep process, readily observable at both levels. An alternate Reynolds decomposition of the instantaneous turbulent fields, using the conditionally averaged signals, allowed the relative importance of large- and small-scale contributions to momentum and heat fluxes to be estimated. The results were found to be in good agreement with comparable studies.

1. Introduction

To a large extent, turbulent transport within and above plant canopies is known to be dominated by large-scale intermittent coherent structures. Their presence in the canopy layer may be revealed by periodic ramp patterns affecting scalar time traces, or more generally speaking, by occasional large-amplitude excursions from the mean on time series of turbulent variables (Raupach *et al.*, 1989; Paw U *et al.*, 1992). They have been observed over a wide range of canopies and turn out to bear a significant contribution to momentum and scalar fluxes, through cycles of 'ejections' and 'sweeps' (Finnigan, 1979; Raupach *et al.*, 1989; Gao *et al.*, 1989; Paw U *et al.*, 1992). A thorough analysis of these coherent motions is a prerequisite to a better understanding of their role on turbulent transport processes.

This paper is the second part of an investigation into the possibilities offered

Boundary-Layer Meteorology **66**: 49–73, 1993.

by the *wavelet transform* for extracting information on turbulence structure in the vicinity of plant canopies, from time series of wind velocities and scalars. The wavelet transform was introduced in the first part (Collineau and Brunet, 1993, hereafter referred to as 'Part I'), as a local transform providing a time-frequency representation of a given signal by a specific wavelet function. After the main mathematical properties of wavelet functions and transform were given, and the principles of wavelet analysis set out, we presented various applications relevant to our purpose. The wavelet variance was shown to provide an estimate of the mean duration of periodic isolated events. The ability of the wavelet transform to detect sharp edges in time series (such as the sudden breakdown of a scalar ramp) was also demonstrated, thereby opening the possibility of using wavelets to perform conditional sampling. The intercomparison of several wavelet functions, using simple artificial data of particular shapes, led us to define a specific range of applications for each of them. In what follows, the reader is supposed to be familiar with the concepts and notations used in Part I.

The aim of the present paper is to apply to real turbulence data the methodology developed in Part I, with the overall aim of gaining insight into how coherent motions affect turbulent transport processes in plant canopy flows. Data acquired in a 13.5 m high pine forest in southwestern France, provide simultaneous time series of wind velocities and air temperature at two levels, under moderately unstable conditions.

After describing the experimental data set, we shall first deduce characteristic time-scales from the wavelet variance. In a second step, the methodology of jump detection will be discussed and the wavelet approach compared with more classical detection techniques such as VITA and WAG; this will provide an estimate of the frequency of occurrence of large-scale motions, over several contiguous hours of data. Conditional averaging will then be performed on the various time series recorded at both levels, allowing the large-scale patterns of the flow to be extracted and ensemble-averaged, and providing details on the dynamics of the ejection-sweep process. Finally, a triple Reynolds-type decomposition of the instantaneous turbulent field, using the conditionally averaged variables, will allow the relative importance of large- and small-scale contributions to momentum and heat fluxes to be estimated.

2. Site and Data

The experiment was carried out in a 20 year old pine forest (*Pinus pinaster Ait.*) in Les Landes area in southwestern France (44° 42′ N, 0° 46′ W) in summer 1989. The height of the canopy h was 13.5 m; the forest was planted in a regular array with 4 m between adjacent rows and 3 m between trees in the same row. Prevailing wind directions yield a fetch of approximately 1 km.

The site was equipped with a 20 m tower, on which were mounted two three-dimensional sonic anemometers/thermometers (Dobbie Instruments, model

TABLE I

Turbulence statistics over eight adjacent half-hour runs (day 250) at levels 1 ($z/h = 1.24$) and 2 ($z/h = 0.82$). h stands for canopy height and z for height above the ground; u and w are the streamwise and vertical windspeed components (m/s), T the air temperature (°C), L the Monin–Obhukhov length (m); overbars mean time averages

Day 250	$\bar{u}_1$	$\bar{T}_1$	$\overline{u'w'_1}$	$\overline{w'T'_1}$	$\bar{u}_2$	$\bar{T}_2$	$\overline{u'w'_2}$	$\overline{w'T'_2}$	h/L
10:00	2.21	24.57	−0.57	0.38	0.89	25.87	−0.39	0.16	−0.157
10:30	2.62	25.30	−0.78	0.42	1.05	26.66	−0.59	0.20	−0.109
11:00	2.79	26.31	−0.71	0.35	1.04	27.67	−0.60	0.25	−0.104
11:30	3.37	26.68	−1.22	0.51	1.24	28.04	−0.87	0.35	−0.067
12:00	2.94	27.14	−1.12	0.54	1.10	28.53	−0.89	0.41	−0.080
12:30	3.17	27.34	−0.99	0.38	1.05	28.71	−0.64	0.25	−0.068
13:00	2.98	28.02	−1.00	0.51	1.02	29.51	−0.67	0.38	−0.089
13:30	2.69	28.21	−0.75	0.39	0.96	29.54	−0.49	0.28	−0.106

PAC100), five one-dimensional sonic anemometers/thermometers (Campbell Scientific Inc., model CA27), and twelve low-frequency sensors for wind speed and air temperature profiles (cup anemometers and double shielded aspirated thermometers).

The present study involves only the measurements made on September 7 (day of year 250) with the 3-D sonic anemometers, at a time when they were located at 16.70 m ($z/h = 1.24$, hereafter referred to as level 1) and 11.05 m ($z/h = 0.82$, level 2) respectively, the lower level corresponding to the bulk of the pine crown. The data were recorded at 16 Hz; a cosine correction was performed on the wind components, which were then rotated to force the lateral wind speed component to zero. A second rotation to force $\bar{w}$ to zero was not performed, except for calculating the mean vertical fluxes $\overline{w'T'}$ and $\overline{u'w'}$. In what follows, u, v and w stand for the streamwise, lateral and vertical wind components, respectively, and T for air temperature. For this study, a period of four hours was selected, corresponding to small rotation angles and slightly unstable conditions. The statistical moments of interest were integrated over 30 min and are displayed in Table I. For coherent motion purposes, the raw data were smoothed and compacted with a sliding window of length 0.5 s. A typical example of u', w' and T' time traces (where the primes denote fluctuations from the 30 min averages $\bar{u}$, $\bar{w}$ and $\bar{T}$) showing clear ramp patterns is shown in Figure 1, along with the instantaneous cross-products $u'w'$ and $w'T'$.

3. Using the Wavelet Transform in Turbulence Studies

In most cases coherent motions yield ramps in scalar time traces (Paw U *et al.*, 1992), that can be seen in Figure 1 for temperature.

The difficulty in detecting these discontinuities accurately comes from the plethora of scales at which they occur, and also from the inevitable background

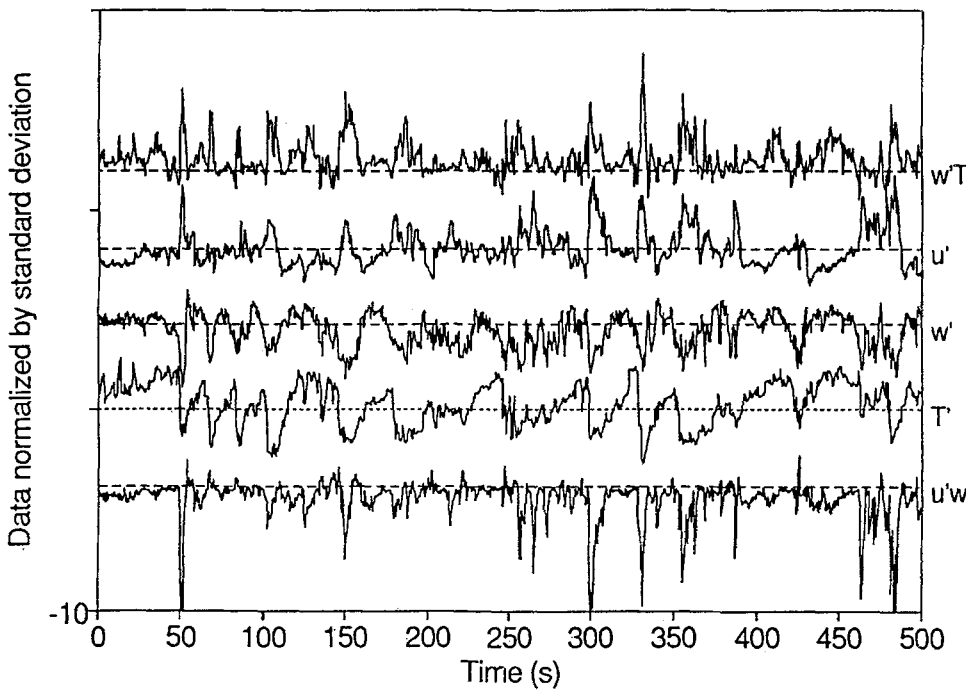

Fig. 1. A sample of time traces of u, w, T, uw and wT at $z/h = 0.82$ (day 250, 10:20). Original data were smoothed by a sliding window of length 0.5 s.

turbulent noise. As discussed in Part I, the filtering properties of the wavelet transform may be able to smooth turbulence signals without erasing the relevant discontinuities. The tenet of wavelet-based detection techniques is recalled in Section 3.2 of the present paper.

The size-detection capability of wavelets has been demonstrated for artificial patterns (Part I) and will be applied to turbulence data to infer a characteristic scale.

3.1. DURATION OF EVENTS

Evidence of the ability of the wavelet variance to determine a mean duration of dominant events was given in Part I, for simple artificial data. We assume that this approach can be extended to experimental turbulence data such as those presented here, featuring a high "signal-to-noise" ratio (signal referring in this case to large-scale excursions from the mean). For this, we computed the wavelet variances over the relevant traces for the first half-hour, using the MHAT wavelet. All scalograms are presented in Figure 2a (u, w and T) and 2b (uw and wT), for both levels. Wavelet variances of wind velocities and cross-products have only one peak, whereas for temperature a secondary peak is visible at large values of the dilation factor. This is due to the existence of slow trends in the temperature

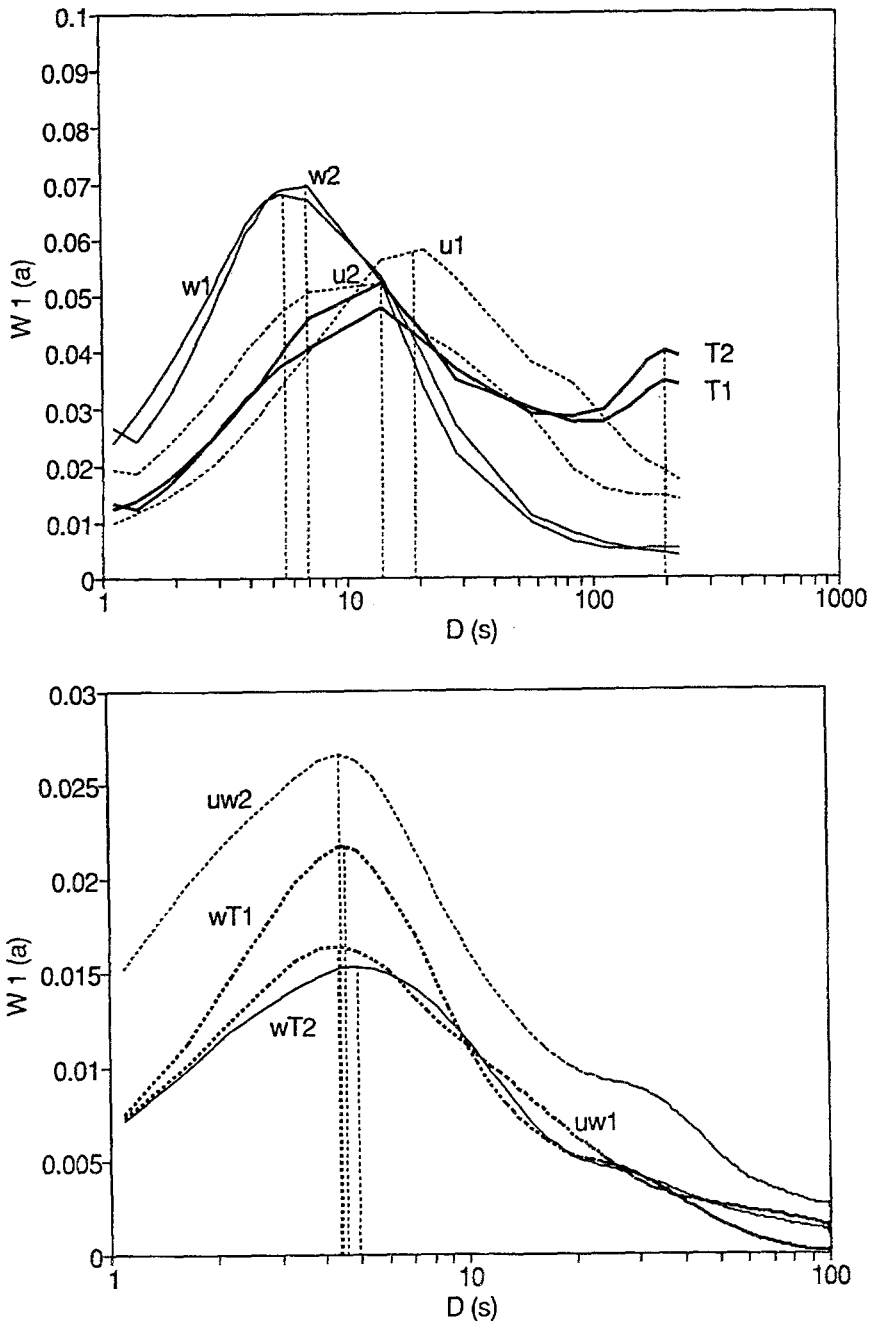

Fig. 2. Wavelet variance scalograms of (a) u, w, T, and (b) wT, uw at $z/h = 1.24$ and at $z/h = 0.82$, calculated with the MHAT wavelet, and plotted as functions of the duration scales D. Indices 1 and 2 refer to $z/h = 1.24$ and 0.82 respectively (day 250, 10:00–10:30).

signal, visible on the sample shown in Figure 1 and probably linked with the presence of intermittent clouds.

Duration scales D were then calculated after identification of the peak scales a_0. We obtained 20, 5.5 and 13 s above the canopy for u', w' and T' respectively, 13, 7 and 13 s within the canopy. The interpretation of these results depends on the nature of the data. For temperature, D certainly corresponds to a mean ramp duration representative of all the ramp-like events clearly visible in the time traces (Figure 1). For u' and w', the situation is more complicated in the sense that it is more difficult to separate visually large-scale structures from smaller-scale turbulence. At both levels, D for w' is about half the value found for T' and is very similar to the duration scale calculated on $u'w'$ and $w'T'$ traces, of the order of 4–6 s at both levels. It is interesting to note that the time traces of the cross-products, or instantaneous fluxes, show very sharp activity around the breakdown time of temperature ramps; at the same time, w' switches rapidly to strong negative values. It therefore seems that these scales are associated with the energetic part of these strong downward motions often referred to as gusts. The duration scale for the streamwise velocity seems to be more related to that of T': they are equal at $z/h = 0.82$ but the reason why a value as large as 20 s is obtained for u' above the canopy is unclear. It may be due to the presence of low frequencies, observable on the u_1 spectra.

In what follows, and in particular for detection purposes, we have used mainly the temperature traces since they show features that are easier to interpret. For reasons developed below, it was then necessary to calculate D for each of the eight runs. As can be seen in Table III, the values found thereby are fairly constant and, on average, equal at both heights (12.2 s at $z/h = 1.24$ and 12.4 s at $z/h = 0.82$).

3.2. Jump detection

Many empirical methods have been used to detect the sharp drops associated with the ramps, the most popular being the Variable Interval Time-Averaging (VITA): all these techniques require the choice of a threshold (Phong-Anant *et al.*, 1980; Schols, 1984; Shaw *et al.*, 1989). In Part I, jump detection algorithms based on wavelets were presented. Wavelet-based methods take advantage of the time-and-frequency representation of wavelets for triggering particular events in data sets. Developments about time- or frequency-localization involving tests on artificial patterns have been necessary for a better understanding of the use of wavelet transform. In this part, we review the tenet and definition of jump detection techniques.

3.2.1. *Wavelet and Zero-Crossing Methods*

The wavelet-based schemes for detecting jumps in signals were defined and described in Part I. The detection function is given by the wavelet transform $T_1(a_0, b)$

of the signal, used at the scale a_0 corresponding to the peak of the wavelet variance.

At this stage, a distinction has to be made among the wavelets used in Part I between those yielding a zero-crossing at jump points (called second derivative-like operators) such as the MHAT wavelet, and those inducing a peak (called first derivative-like operators) such as the HAAR, RAMP or WAVE wavelets. Detection according to the first type only involves identification of zero-crossing points with a particular slope sign depending on the slope of the jumps. Detection according to the second type will require the use of a threshold to select the larger peaks in the wavelet detection function.

3.2.2. *Classical Methods*

The two following classical methods are considered as reference schemes. The first one, VITA, has been much used by turbulence researchers (Subramanian *et al.*, 1982; Bogard and Tiederman, 1986; Schols, 1984; Shaw *et al.*, 1989). The VITA technique involves a short-term variance of temperature data, calculated on a time interval Δt corresponding to durations less than the time between adjacent events and normalized by the long-term variance:

$$\mathrm{VITA}_{\Delta t}(t) = \frac{1}{\sigma_T^2}\left[\frac{1}{\Delta t}\int_{t-\Delta t/2}^{t+\Delta t/2}[T'(t)]^2\,\mathrm{d}t - \left[\frac{1}{\Delta t}\int_{t-\Delta t/2}^{t+\Delta t/2}T'(t)\,\mathrm{d}t\right]^2\right]. \tag{1}$$

Thus, the VITA scheme is able to detect the sharp drops ending the temperature ramps, where it exhibits positive peaks. It actually behaves like a low-pass filter limited by the frequency $1/\Delta t$. We use an additional negative slope criterion to discriminate sharp decreases from increases. Then the detection occurs when the VITA function exceeds a certain threshold k, provided that the slope of the temperature trace is negative.

The Window Averaged Gradient (WAG) technique (Bisset *et al.*, 1990) is very similar to VITA, except that it is based on the first-order moment instead of the variance. It detects jumps by translating in time a differential scheme made by the difference between a short-term mean before and after the instant considered:

$$\mathrm{WAG}_{\Delta t}(t) = \frac{1}{\sigma_T}\frac{1}{\Delta t}\left[\int_{t-\Delta t/2}^{t}T'(t)\,\mathrm{d}t - \int_{t}^{t+\Delta t/2}T'(t)\,\mathrm{d}t\right]. \tag{2}$$

This technique is able to separate sudden decreases from sudden increases without any additional slope criterion. The detection point is the time at which WAG exceeds a threshold k, as before with VITA.

The Δt and k parameters of the VITA and WAG techniques have to be cali-

brated: this will be done here as is usual by matching the total number of detected events with a reference set.

4. Evaluation of Detection Algorithms According to the Period Between Events

In this part, our purpose is to evaluate detection techniques according to their ability to estimate Δ, the mean time-interval between events. The evaluation is performed on a single half-hour set of data (day 250; 10:00–10:30) within the canopy with six techniques: VITA, WAG, HAAR, RAMP, WAVE, MHAT. Since all these techniques are jump-detectors, they are applied to air temperature data. The zero-crossing method (involving the MHAT wavelet) can however be easily implemented either on T' and u' time series, since it does not require a calibration. The results are to be compared to a reference set of ramp events.

4.1. Calibration and comparison of methods

All jump detection techniques need to be calibrated with respect to one or two parameters: the scaling parameter for the wavelet methods (chosen *a priori* as the wavelet variance peak scale a_0), a threshold for the first derivative-like wavelets, the window width and a threshold for VITA and WAG.

Because none of these methods can be considered as a genuine reference, we have visually selected a reference set of detection points based on the identification of temperature ramps. As pointed out by Paw U *et al.* (1992), visual identification of turbulent coherent structures is indeed considered by most researchers as the method by which all other detection methods are checked and validated. This reference set consists of 60 events over the 30 min period chosen (day 250; 10:00–10:30). Following Subramanian *et al.* (1982) and Bogard and Tiederman (1986), the adjustment of the parameters (time integral for classical methods, thresholds when needed) has been performed under the requirement of getting a number of events closest to 60.

Figure 3 shows on the same graph the wavelet variance for the zero-crossing method and the number of events detected, as a function of the duration scale D. As expected, the number of detections decreases with D, since a wavelet with a large dilation factor can only detect the largest events. In other words, wavelets look at data at a particular scale, necessitating the choice of an optimal scale. It is precisely on this point that an important result is obtained: with the scale a_0, corresponding to the variance peak, the number of events detected is 62, very close to the reference value of 60. Furthermore, it is shown below that these events are, to a good approximation, the same as those selected visually, with few extra or missing detections. This, again, lends strong support to the assumption made in Part I, according to which the wavelet variance approach, successfully tested on simple patterns of equal length, may also be valid for real turbulence data showing large excursions from the mean, but also featuring a wide range of scales.

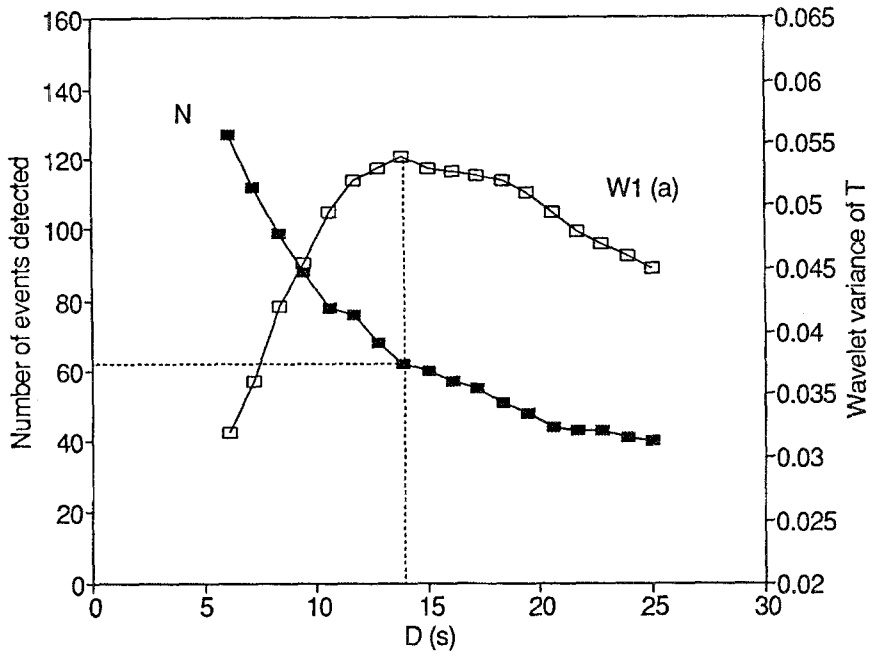

Fig. 3. Effect of the dilation parameter on the number of events detected (day 250, 10:00–10:30, $z/h = 0.82$), using MHAT.

For the other five methods, the choice of parameters is obviously dramatic, as pointed out by Bogard and Tiederman (1986) who discussed the effect of thresholding. The adjustment procedure gave the following threshold values for the first derivative-like wavelets: 0.2 for HAAR, 0.15 for RAMP, and 0.55 for WAVE. A calibration based on Δt-values ranging from 2 to 20 s also gave the VITA and WAG parameters: respectively $\Delta t = 10$ s and $k = 0.55$; $\Delta t = 8$ s and $k = 0.6$. The outputs of the VITA and WAG techniques appear reasonably stable in this range of parameters.

Figure 4 shows a 500 s subset of the original temperature data, together with the six detection functions and all detection times. The total number of events detected in each case is given in Table II; it is of course close to 60 since all methods were first calibrated (except MHAT already discussed).

The question now arises as to whether the different schemes have selected the same events. Table II also shows the probability P(Ref) of detecting the reference events, and the probability P(Err) of wrong detections for each technique. Discrepancies in VITA (28% of wrong detections) often come from multidetection of a single event (see Figure 4). First derivative-like wavelet methods (Figure 4) show acceptable (HAAR, RAMP) to very good agreement (WAVE) with the reference frame. It has to be pointed out that the WAVE wavelet has the localization in frequency of Gaussian derivatives and not the tendency to extra detections

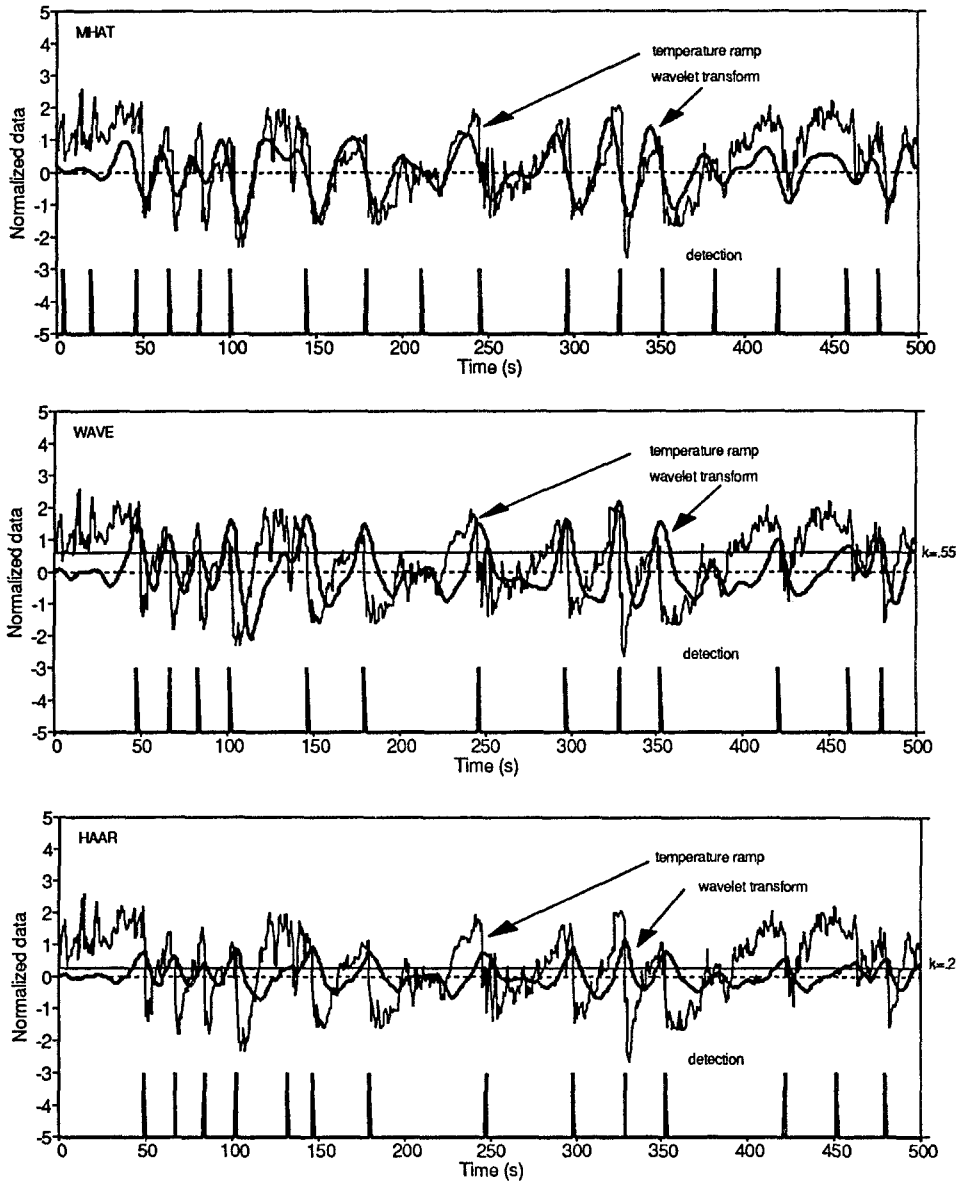

Fig. 4(a–c).

of zero-crossings discussed below. However, it needs a threshold calibration, which is often subjective for routine applications. Errors in zero-crossings (MHAT) are due to too good a localization in frequency of the Laplacian of a Gaussian: this method misses very close events, while it tends to add irrelevant events during quiescent periods with no referenced events (see the beginning of time-series in

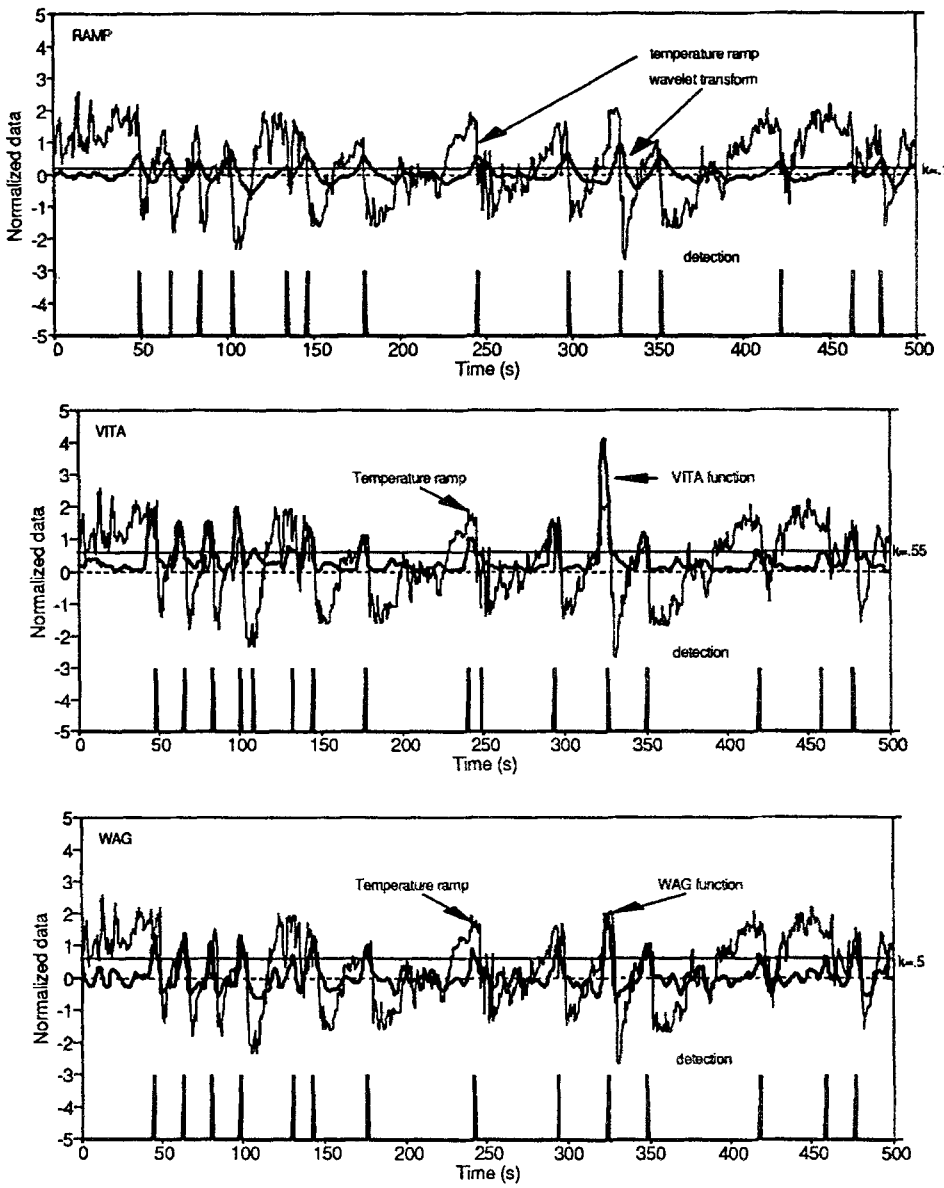

Fig. 4(e–f). Wavelet detection functions for temperature data (day 250, 10:00–10:30), using (a) MHAT, (b) WAVE, (c) HAAR, (d) RAMP, (e) VITA, (f) WAG.

Figure 4). This is a consequence of very variable time-intervals between events on a method well localized in frequency. However, it is fortunately limited to a few false detections per half-hour, so that the zero-crossing technique, easier to implement, can be considered as efficient on turbulence data. It is interesting to

TABLE II

Results of the detection schemes for the first run (10:00–10:30) of day 250, at $z/h = 0.82$. P(Ref) is the probability of detecting the reference events, P(Err) the probability of wrong detections and N the number of events detected by each technique

Detection technique	Data	Δt (s)	D (s)	k	P(Ref) %	P(Err) %	N
VITA	T'	8.0	–	0.55	66	28	63
WAG	T'	10.0	–	0.60	83	17	62
HAAR	T'	–	13.0	0.20	88	17	59
RAMP	T'	–	11.0	0.15	87	17	60
WAVE	T'	–	14.0	0.55	93	12	58
MHAT	T'	–	14.0	–	88	12	62
MHAT	u'	–	15.0	–	90	17	58

note that the results obtained with the u' signal turn out to be as good as those obtained with T'.

4.2. Interpretation

One important result obtained from the set of detected points is Δ, the mean time-interval between events. Figure 5a shows an histogram of the corresponding time-intervals between the events selected by the zero-crossing technique: it peaks at about 30 s with 75% of the results in the range 20–35 s. Time-interval distributions for classical (VITA and WAG) or even first derivative-like wavelet methods resemble an exponential law (Bogard and Tiederman, 1986), because threshold methods at small scales lead to multidetection of single events, so that the corresponding histogram of time-intervals is more weighed towards the smallest time-intervals and, in many cases, does not exhibit characteristic peaks. Precision in the peak values is eventually influenced by the time localization of techniques and false or missing detections. The zero-crossing technique realizes a trade-off between these effects.

Given the scatter observed on these histograms, one can question the statistical significance of Δ. Figure 5b presents a chronological display of the time-intervals between events from a half-hour set (day 250, 10:00–10:30, 60 events for 30 min): in such a representation, peaks correspond to long quiescent periods without events. One cannot deduce any unimodal periodic behaviour. Instead, series of consistent events (of period 20–25 s) are followed by "quiescent" periods (of about 100 s), but no steady regime can be determined. Thus a mean value of 29 s gives a very crude idea of the processes involved with a standard deviation of 11 s.

5. Evaluation of Detection Algorithms According to the Averaged Patterns

Detection techniques used in Section 4 have shown their ability to detect characteristic ramp-events. This now allows one to perform conditional averages of the

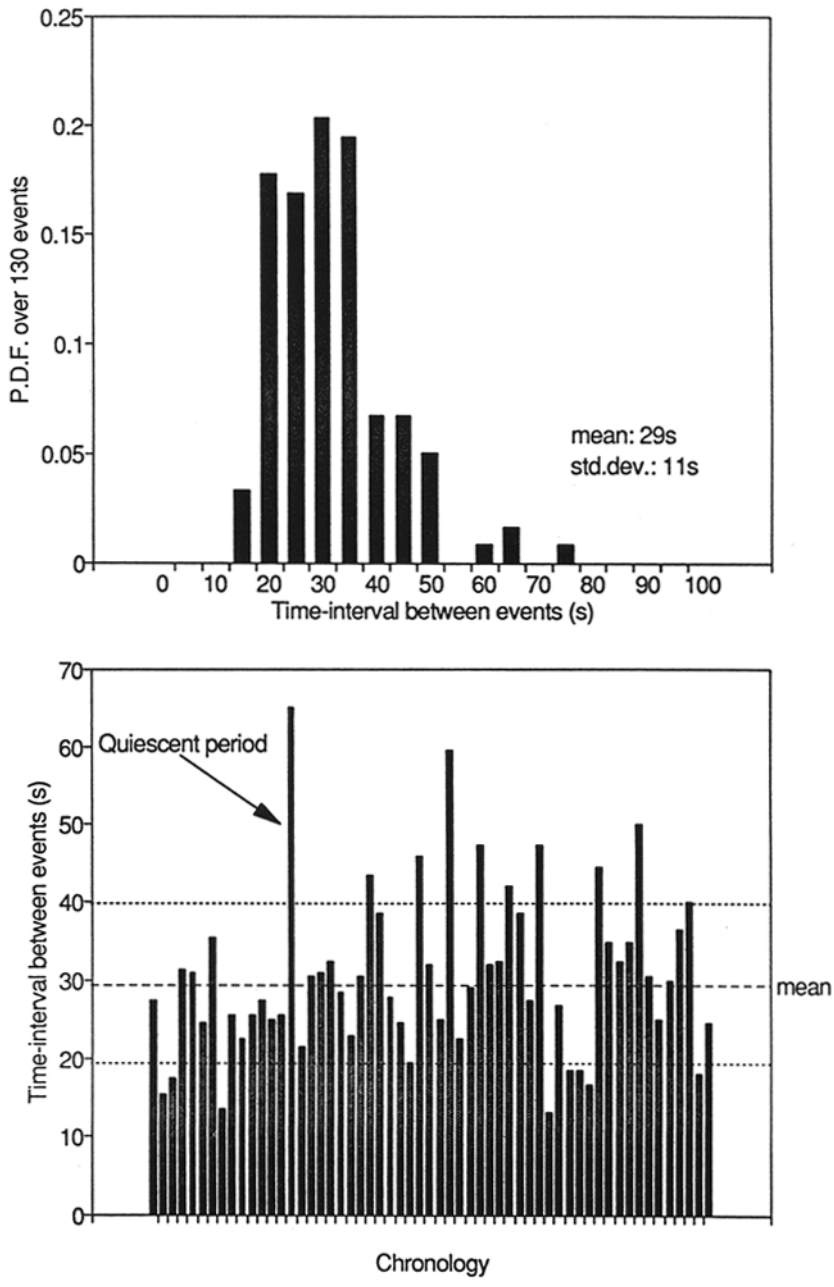

Fig. 5. (a) histogram (day 250, 10:00–11:00) and (b) chronological display (day 250, 10:00–10:30) of time-intervals between events for the zero-crossing technique applied on temperature data.

turbulent fields around particular times. Conditional averages have been used by several researchers, using principally VITA (Phong-Anant *et al.*, 1982; Schols, 1984); Subramanian *et al.* (1982) have compared different techniques, and concluded that there are significant technique effects, especially for second-order moment averaging. Thus, the methods used in Section 4 have to be intercompared with respect to pattern averaging.

We conditionally sample and average the wind speed components and temperature as well as their second-order moments. For each detection scheme, conditional averages are sampled on a 30 s long window centered at detection points. For techniques involving thresholds, the detection point is given by the instant corresponding to the peak of the detection function for each occurrence. With the zero-crossing method, the zero-crossing instant defines the center of the window. The length of 30 s chosen for the averaging window is of the order of the period between events. Brackets will be used for conditional averages of a function f and N for the total number of detected events, so that:

$$\langle f(t)\rangle = \frac{1}{N}\sum_{i=1}^{N} f(t+t_i) \quad (t \in [0, 30\,\text{s}),\ t_i \text{ is the detection time}). \tag{3}$$

This definition requires no other assumption than those included in the detection scheme. From such a basic definition, one would expect rather variable results; as a matter of fact, factors such as the variability of size of the events and the uncertainty in time and scale of the detection schemes all tend to reduce their accuracy and clarity. As far as conditional averaging is concerned, localization-in-time properties appear very important, because the uncertainty in conditional averages depends on the time at which the averaging window is centered. From Part I, we know that the RAMP and HAAR wavelets are well localized in time, whereas MHAT and WAVE are well localized in frequency. However, it turns out that results exhibit quite clear and repeatable features, whatever the wavelet function.

5.1. A QUALITATIVE AGREEMENT BETWEEN TECHNIQUES

Let us first of all investigate the effect of the choice of the detection scheme by comparing the six techniques presented above. Here, the techniques are compared on the same data as in Section 4. The detection is also performed on air-temperature traces. In Figure 6 conditional averages are compared of first- and second-order moments normalized by their standard deviations calculated over the 30 min.

In addition to the uncertainty of detection techniques, the degradation of accuracy, as distance from the detection point increases, may also come from the variability of both the duration and the period between events, which can lead to overcrossings between adjacent events.

In order to investigate the statistical significance of conditional averages, we present in Figure 7 standard deviations at each point of the window for temperature

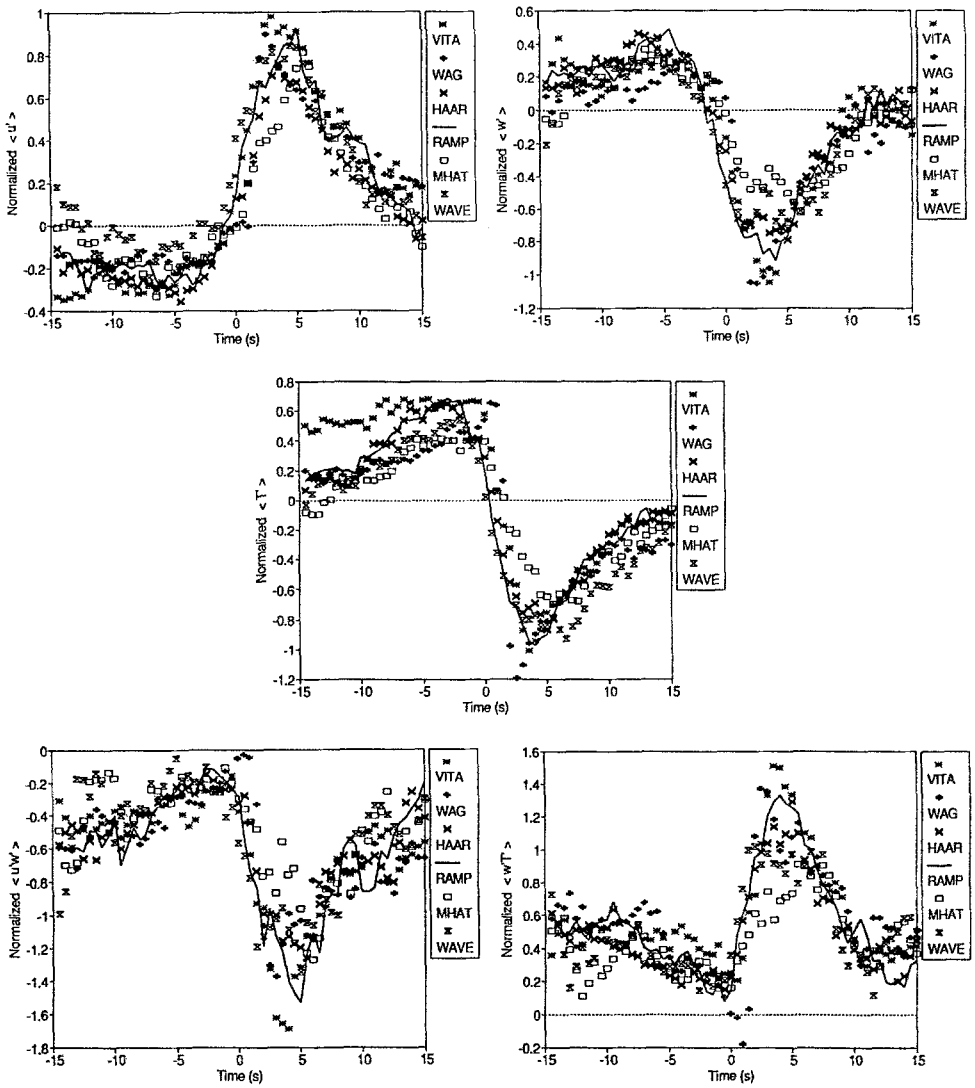

Fig. 6. Conditional averages of u, w and T (normalized by their respective standard deviation) and uw, wT (normalized by their respective standard deviation) at $z/h = 0.82$ with the 6 detection schemes (day 250, 10:00–10:30, z/h = 0.82).

data (it would be similar for other turbulence fields). Such high variability, even if expected from a visual observation of data, has to be kept in mind in the following interpretations of conditional averages.

5.2. Comparison of techniques

Given this overall agreement, three criteria have been used to evaluate the techniques: first, the sharpness of the temperature ramps retrieved; second, the step

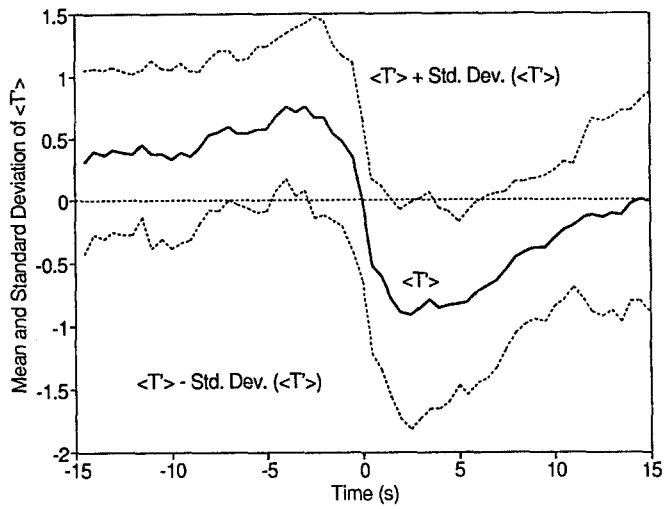

Fig. 7. Mean and standard deviations of conditionally averaged temperature data, using RAMP ($z/h = 0.82$, day 250, 10:00–10:30). Data are normalized by their standard deviation.

size; and, third, the duration of the events. Since temperature ramps are chosen to diagnose the presence of coherent motions, the sharpness observable after the averaging process characterizes the ability of each technique to perform a good localization in time. This is the key point in conditional averaging, especially if quantitative information upon duration or amplitude scales is needed.

In Figure 6, the collection of curves remains within a reasonable range. However, because of the weak localization in time of the associated wavelet, the sharpness of the peaks obtained from the zero-crossing method is less marked. The jump excursions, normalized by the corresponding standard deviations, range from 1.1 to 1.7. This is less than what can be observed for single events in time series (peak values up to 2–3, as observable on Figure 1), because of the effect of the averaging procedure itself. WAVE and MHAT yield lower step sizes.

The mean event durations, visually determined from the averaged patterns, match correctly the values obtained from the wavelet variance peaks, despite a tendency to be slightly longer because of the degradation noticed at the jumps of the averaging window. The VITA results, especially for temperature averages, yield longer durations that may be due to multidetections of single events.

Thus, WAG, HAAR and RAMP are the most successful averaging techniques, given their good localization in time. In what follows, all conditional averages will be performed by the RAMP method.

6. Run-to-Run Consistency of the Results

In this rather methodological work, we have so far focused on a single run of data (day 250, 10:00). The question arises now as to whether the same results would

TABLE III

Number of events N_1 and N_2 detected at levels 1 and 2 from the zero-crossing method applied on temperature data, and characteristic duration scales D (s) calculated from the wavelet variance for 8 adjacent half-hour runs (day 250)

	10:00	10:30	11:00	11:30	12:00	12:30	13:00	13:30
N_1	71	84	56	66	50	79	76	68
N_2	62	70	74	69	62	73	68	69
D (T_1)	11.5	11.5	12.0	12.5	17.4	11.0	10.5	11.0
D (T_2)	13.0	12.5	10.0	11.1	14.3	11.5	15.5	11.0
D (uw_1)	4.0	6.0	5.0	2.5	3.5	3.5	4.0	4.0
D (wT_1)	5.0	6.5	5.0	5.0	5.0	5.0	6.5	6.0

be obtained for similar dynamic and thermal conditions. We therefore performed the same analyses over eight contiguous 30 min runs on the same day, under moderately unstable conditions.

Table III presents the results obtained on temperature traces at each level, in terms of the number of events detected and the time scales defined by the wavelet variance. MHAT was used for this particular purpose since it requires no calibration, which is a great advantage when several runs have to be analysed.

The wavelet variance gives a rather stable value for D: about 12 s for temperature at both levels, 4 s for uw_1 and 5.5 s for wT_1. On average, the number of events detected is identical at both levels (69 and 68 at $z/h = 1.24$ and 0.82, respectively), giving a mean interval of 26 s between adjacent events (or $1.8h/u_*$). This number appears very stable at $z/h = 0.82$ but more variable above the canopy, so that a difference up to 14 detections per run can be obtained between the two levels; this is probably due to a more significant number of missed or false detections at $z/h = 1.24$, where the "signal-to-noise" ratio is lower (small-scale turbulence appears more important relative to the magnitude of large-scale structures), as is clearly visible on the traces.

Conditional averaging was then performed on the same runs, using RAMP as a detection scheme. The results obtained on $\langle u' \rangle$, $\langle w' \rangle$, $\langle T' \rangle$, $\langle u'w' \rangle$ and $\langle w'T' \rangle$, are presented in Figure 8 for the eight runs, both above and within the canopy. The patterns extracted appear surprisingly stable for the first- and second-order moments, especially in the canopy; the largest scatter is found on $\langle u' \rangle$, $\langle w'T' \rangle$ and especially $\langle u'w' \rangle$ at $z/h = 1.24$. The remarkable result here is the consistency of the patterns exhibited by the wind speed components and the cross-products from run to run, whereas the detection was only performed on the temperature traces. This suggests the existence of a strong dynamic link between the various traces, which we must now consider in more detail.

7. Averaged Patterns and Turbulent Processes

7.1. Wind field and temperature

In order to get a better picture, the structures extracted from these eight previous

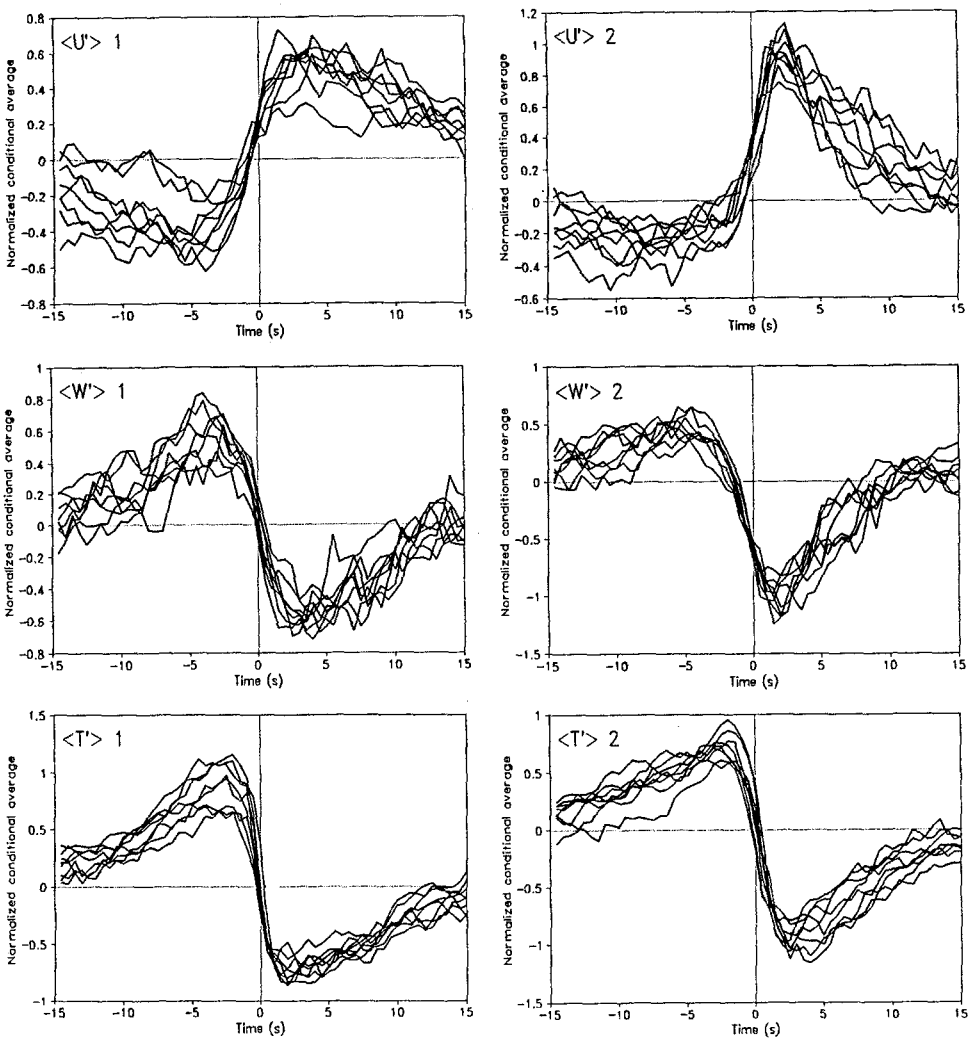

Fig. 8(a).

runs were ensemble-averaged. The first-order moments, still normalized by their respective standard deviations, are shown on Figure 9a, above and within the canopy. Here again, the results are presented over 30 s windows centered at the detection point.

The patterns obtained above the canopy show a characteristic temperature rise, accompanied by a slow ($\langle u' \rangle < 0$) upward ($\langle w' \rangle > 0$) movement of air, followed by a sharp drop (although, of course, smoother here than on the individual structures). Simultaneously, the wind switches to a strong downward motion ($\langle w' \rangle < 0$) associated with an acceleration of horizontal velocity ($\langle u' \rangle > 0$). This two-stage process has already been observed in numerous turbulent laboratory

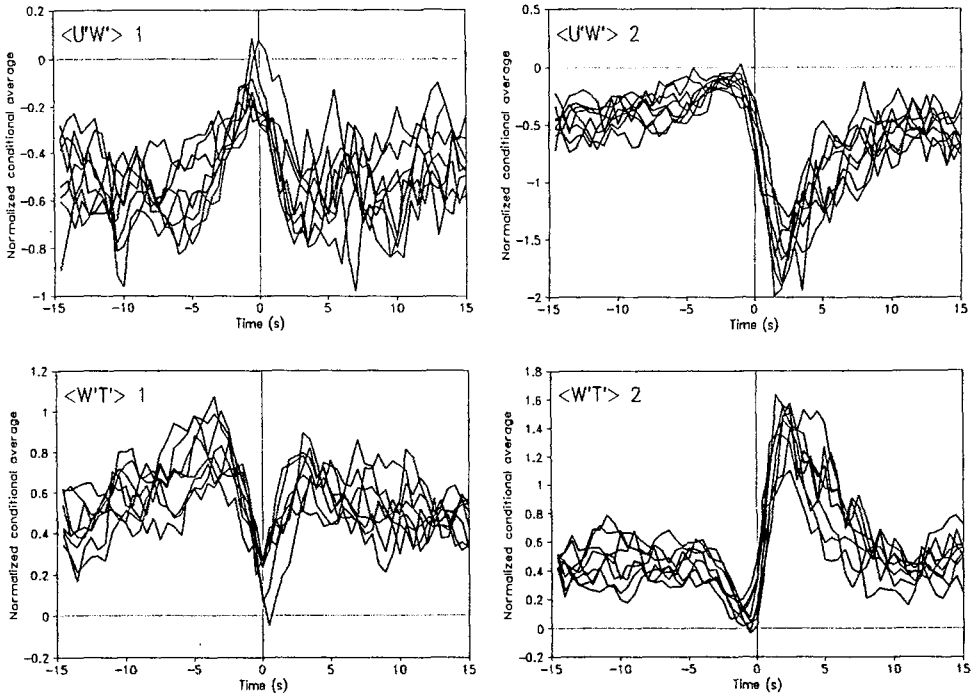

Fig. 8(b). Superimposed conditional averages of (a) u, w and T for 8 adjacent data runs (10:00; 10:30; 11:00; 11:30; 12:00; 12:30; 13:00; 13:30) (left: $z/h = 1.24$; right: $z/h = 0.82$). (b) Same for uw and wT. Data for each run are normalized by the corresponding standard deviation.

and atmospheric boundary layers (e.g., Phong-Anant *et al.*, 1980; Rajalopalan and Antonia, 1982; Shaw *et al.*, 1989; Gao *et al.* 1989; Bergström and Högström, 1989; Paw U *et al.*, 1992), and similar patterns obtained by conditional analysis. The first stage is referred to as an "ejection", or an updraft bringing up air from below (warmer in our case), while the second is a typical "sweep", a downdraft carrying high momentum (cooler) fluid down from aloft. Here, the temperature trace is quite similar to, and in phase with, the vertical velocity trace, whereas the streamwise velocity is out of phase. $\langle u' \rangle / \sigma_u$ and $\langle w' \rangle / \sigma_w$ have the same magnitude (peaking at about ± 0.5) and appear smaller than $\langle T' \rangle / \sigma_T$, which peaks near ± 0.8.

Qualitatively speaking, similar patterns are visible at $z/h = 0.82$. However, the ensemble-averaged traces of first-order moments appear more asymmetric about the detection point within the canopy than above: in the former case, the absolute magnitude of the large-scale fluctuations is significantly higher during the sweep than during the ejection. For instance, the ratio of the maxima reached by $\langle w' \rangle / \sigma_w$ after and before the front is about -1 at $z/h = 1.24$ against -2 at $z/h = 0.82$; the difference is even higher for $\langle u' \rangle$ and $\langle T' \rangle$. This asymmetry is largely responsible for the values reached by the skewness of the distributions in the canopy ($Sk_u = 1.28$, $Sk_w = -0.48$, $Sk_T = -0.23$ at $z/h = 0.82$, on average for the same period

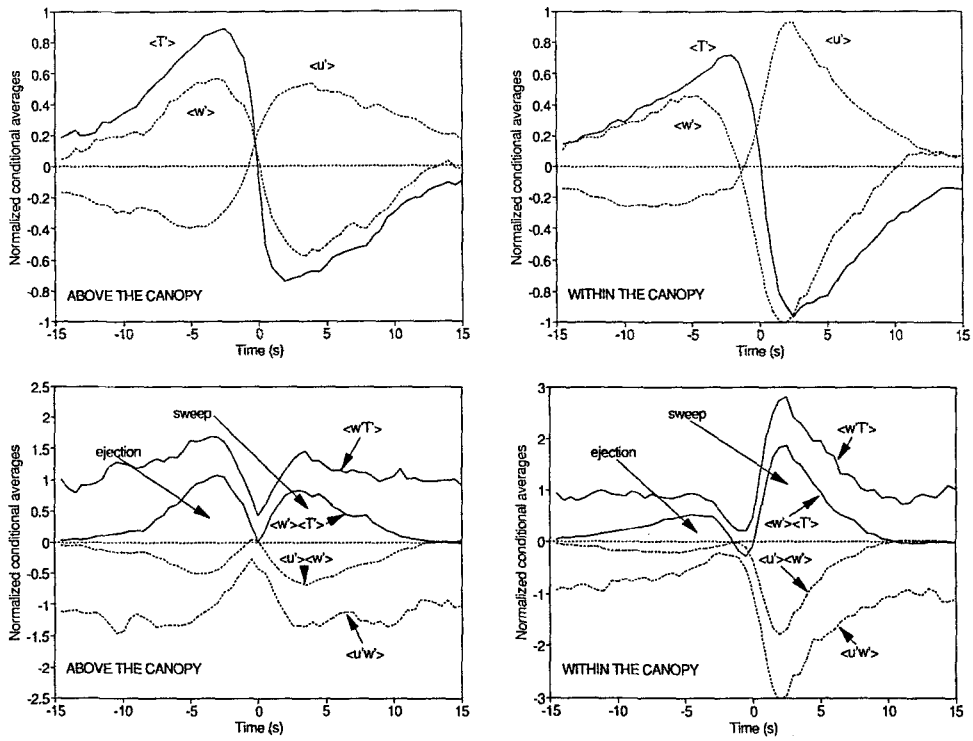

Fig. 9. Superimposed conditional averages of u, w, T, uw and wT, using RAMP on temperature data above the canopy (left) and within the canopy (right). Cross-products $\langle u'\rangle\langle w'\rangle$ and $\langle w'\rangle\langle T'\rangle$ are also displayed. $\langle u'w'\rangle$ and $\langle u'\rangle\langle w'\rangle$, $\langle w'T'\rangle$ and $\langle w'\rangle\langle T'\rangle$ are normalized respectively by $|\overline{u'w'}|$ and $|\overline{w'T'}|$.

of time), showing a higher departure from Gaussian than above ($Sk_u = 0.41$, $Sk_w = -0.16$, $Sk_T = -0.15$ at $z/h = 1.24$).

Another difference between the two heights is the existence of a time lag at $z/h = 0.82$ between temperature and vertical wind speed at the detection time, which is not observable above. This feature happens repeatedly, since Figure 9 shows data averaged over eight half-hour runs. Time lags for maximum correlations were calculated from space-time correlations between the various traces at the two heights, taking the upper level as the reference; the results are displayed in Table IV. One striking result is the absence of any lag between vertical velocities, as already observed by Raupach *et al.* (1989) over a model canopy in a wind-tunnel and in a eucalyptus forest, and by Shaw and Zhang (1992) in a deciduous mixed forest. At the upper level, there is no lag either between temperature and vertical velocity. On the other hand, temperature at $z/h = 0.82$ exhibits a delay of about 1.5 s on average with temperature at $z/h = 1.24$; this leads to a mean normalized value of $\tau U_h/h \approx 0.32$ between these two heights (τ being the delay and U_h the mean horizontal velocity at treetop), in excellent agreement with the

TABLE IV

Time-lags (s) corresponding to maxima in cross-correlations, for eight adjacent runs (day 250)

Delay (s)	10:00	10:30	11:00	11:30	12:00	12:30	13:00	13:30
T_1, T_2	1.50	1.50	1.75	1.00	1.25	1.25	1.00	1.25
w_1, w_2	0.	0.	0.	0.	0.	0.	0.	0.
w_1, T_1	0.	0.	0.	0.	0.	0.	0.	0.
u_1, u_2	1.50	0.	0.75	0.	0.25	0.50	0.	0.50
u_1, T_1	0.50	0.50	0.	0.50	0.50	0.	0.25	0.

observations of Raupach *et al.* (1989) and Shaw and Zhang (1992). A lag also exists between streamwise velocities, although smaller than for temperature; this was observed too by these authors.

Further analysis of the data recorded at other levels, and especially deep in the canopy where negative time lags have been reported for longitudinal velocities, will provide a more complete picture. Generally speaking, these features have been shown by these authors and others to be consistent with the existence of downwind tilted coherent structures (such as double-roller type eddies) containing inclined scalar microfronts, which manifest themselves in the traces as ramp patterns.

7.2. Momentum and Heat Transport

More insight can be gained by examining the flux patterns. For this purpose, it is convenient to use a triple decomposition of the turbulent variables (Antonia *et al.*, 1987; Brunet and Raupach, 1987; Bergström and Högström, 1989). Indeed, any instantaneous variable $F(u, w, T)$ can be decomposed into:

$$F = \bar{F} + f_l + f_s\,, \tag{4}$$

where $\bar{F}$ is the long-term average, f_l a perturbation due to the large-scale motion and f_s the remaining small-scale fluctuation; the sum $f_l + f_s$ is the turbulent fluctuation f' in the conventional Reynolds decomposition. If conditional averaging is applied to $f' = F - \bar{F} = f_l + f_s$, we get $\langle f' \rangle = f_l$ under the assumption that f_s is uncorrelated with the detected large-scale motion ($\langle f_s \rangle = 0$). For a product of two fluctuations f' and g', we also obtain:

$$\langle f'g' \rangle = \langle f' \rangle \langle g' \rangle + \langle f_s g_s \rangle\,. \tag{5}$$

If we now define an averaging operator $\langle \tilde{} \rangle$ at the scale of the detection window, such that:

$$\langle \tilde{f} \rangle = \frac{1}{\Delta T} \int_{-\Delta T/2}^{+\Delta T/2} \langle f'(t) \rangle \, \mathrm{d}t\,, \tag{6}$$

where ΔT is the window width (30 s here), and perform this average on Equation (5), we obtain:

$$\langle \widetilde{f'g'} \rangle = \langle \widetilde{f'} \rangle \langle \widetilde{g'} \rangle + \langle \widetilde{f_s g_s} \rangle . \tag{7}$$

If the window is representative of the mean period of the motion (i.e., if the structures detected are reasonably representative of the flow), then $\langle \widetilde{f'g'} \rangle$ should be close to the conventional Reynolds-averaged flux $\overline{f'g'}$, and the first term on the right-hand side of Equation (7) represents the contribution to $\overline{f'g'}$ from the organized motions.

Figure 9b shows the ensemble averages of the products $\langle u'w' \rangle$ and $\langle u' \rangle \langle w' \rangle$ (normalized now by the total flux $|\overline{u'w'}|$), as well as $\langle w'T' \rangle$ and $\langle w' \rangle \langle T' \rangle$ (normalized by $\overline{w'T'}$), both above and within the canopy. First of all, $\langle \widetilde{u'w'} \rangle / \overline{u'w'}$ and $\langle \widetilde{w'T'} \rangle / \overline{w'T'}$, calculated from the digital time series over the window, are found to be reasonably close to 1 (respectively, 1.11 and 1.15 at $z/h = 1.24$, and 1.12 and 1.11 at $z/h = 0.82$). Given the uncertainties associated with the measurements, the detection process and the assumption leading to Equation (5), this shows that the value chosen for the window length provides a fairly correct representation of the flow. Using the same procedure, Antonia and Fulachier (1989) obtained values of 0.93 and 1.13 for shear stress and heat flux, respectively, in a turbulent laboratory boundary layer.

Ejections and sweeps are clearly visible on the traces, and provide two distinct contributions to the overall fluxes. The ratio of the total stress fraction transferred by sweeps to that transferred by ejections is found to be 1.04 at $z/h = 1.24$ against 2.43 at $z/h = 0.82$. These values are consistent with results from quadrant analysis reported by Shaw *et al.* (1983) over corn (about 1.5 and 2.5), and Finnigan (1979) over wheat (about 2.0 and 3.5 at similar heights). Slightly smaller ratios are obtained here for sensible heat flux: 0.89 at z/h=1.24 and 1.82 at z/h=0.82. It has to be pointed out that conditional analysis thus provides not only quantitative results on the relative importance of sweeps and ejections, as does quadrant-hole analysis, but also insight into the *dynamics* of the processes, since part of the temporal information is conserved.

The large-scale contributions to fluxes, $\langle \widetilde{u'} \rangle \langle \widetilde{w'} \rangle / \langle \widetilde{u'w'} \rangle$ and $\langle \widetilde{w'} \rangle \langle \widetilde{T'} \rangle / \langle \widetilde{w'T'} \rangle$ are found to be, respectively, equal to 0.26 and 0.40 at $z/h = 1.24$ and 0.31 and 0.39 at $z/h = 0.82$. It is interesting to note that large-scale motions appear to be more efficient at transporting heat than momentum, which was also noticed by Antonia *et al.* (1987) and Antonia and Fulachier (1989).

Gao *et al.* (1989) obtained values as high as 0.75 for heat and momentum transfer near a deciduous forest top by sampling the downdrafts and updrafts associated with a series of 18 temperature ramps identified by eye, the traces being filtered with a 10 s running average in order "to reduce the background turbulence". The origin of the difference between these results is not clear. *A priori*, one can question the (subjective) visual selection of Gao *et al.* (1989), which may tend to favor the largest events, as well as their procedure to remove small-scale motions.

One may also question the validity of the assumption required to obtain our

Equation (5). Concerning this point, one notices on Figure 9b that the small-scale contribution to the fluxes, seen at all times as the difference between $\langle f'g' \rangle$ and $\langle f' \rangle \langle g' \rangle$, appears as a roughly constant background level, although it tends to increase towards the edges of the windows. In this sense, the assumption of small- and large-scale motions being uncorrelated is not entirely appropriate but seems reasonable enough for our purpose.

Furthermore, it is important to notice that our findings are in good agreement with other reported studies based on a similar triple decomposition of the turbulent variables. For example, Antonia *et al.* (1987) obtained typical values of 0.28 and 0.44 in the turbulent far wake of a cylinder, for the large-scale contributions to momentum and heat fluxes, respectively. In other words, this type of result may depend substantially on the detection and averaging procedures, and further work is obviouly needed to clarify this.

8. Concluding Discussion

Two types of results have been presented in this paper: firstly, methodological results on the wavelet approach itself, when applied to real turbulence data; secondly, results concerning the nature of turbulence in a forest canopy.

One of the remarkable results of the first type is the efficiency of wavelets at detecting jumps in turbulent time series; a quite satisfying correspondence was obtained between the large structures initially selected by eye on a reference time trace and the events detected by the four wavelets used. The zero-crossing method is particularly interesting since it requires no empirical calibration.

Detection being performed on temperature only, conditional averaging allowed a representative pattern to be extracted for each turbulent variable, and for the cross-products representing vertical transfer. These patterns turned out to be remarkably stable throughout a period of four hours. Noticeable differences were found on first-order moments between the two measurements levels, accounting for the differences in the skewnesses of these variables, and for the dominance of sweeps over ejections in the canopy, readily visible on the cross-product patterns.

More generally, the approach followed in this paper appears able to provide substantial information on the dynamics of turbulent transport processes. In particular, the triple decomposition we used allowed the relative importance of small-scale mixing (appearing here at a fairly constant background level) and motions due to coherent structures to be evaluated fairly simply, on average as well as on an instantaneous basis.

This work is to be considered more as a methodological study than a complete analysis: we restricted ourselves to a few hours of data acquired under similar flow conditions. In particular, no attempt was made to investigate the possible dependency of the frequency of occurrence of coherent structures on characteristic flow variables such as u_*, U_h or z/L. Indeed, Raupach *et al.* (1989) showed that the gust frequency should be a function of a shear scale u_*/h, which was subsequently

confirmed by Paw U *et al.* (1992) on several sets of canopy data. Here, only a mean value for gust frequency was obtained ($0.56u_*/h$). This needs further work and is obviously one of the major goals attainable through the use of wavelet analysis.

Acknowledgments

Dr Paul Berbigier, Dr Adama Diawara and Daniel Poudroux are gratefully acknowledged for their collaboration during the Landes experiment, which was partially supported by a grant from the Institut National des Sciences de l'Univers. The authors are indebted to Dr D. Baldocchi, R. Valigura and R. Hosker for their comments on an early draft of the manuscript.

References

Antonia, R. A., Browne, L. W. B., Bisset, D. K., and Fulachier, L.: 1987, 'A Description of the Organized Motion in the Turbulent Far Wake of a Cylinder at Low Reynolds Number', *J. Fluid Mech.* **184**, 423–444.

Antonia, R. A. and Fulachier, L.: 1989, 'Topology of a Turbulent Boundary Layer with and without Wall Suction', *J. Fluid Mech.* **198**, 429–551.

Bergström, H. and Högström, U.: 1989, 'Turbulent Exchange above a Pine Forest, II. Organized Structures', *Boundary-Layer Meteorol.* **49**, 231–263.

Bisset, D. K., Antonia, R. A., and Browne, L. W. B.: 1990, 'Spatial Organization of Large Structures in the Turbulent Far Wake of a Cylinder', *J. Fluid Mech.* **218**, 439–461.

Bogard, D. G. and Tiederman, W. G.: 1986, 'Burst Detection with Single-Point Velocity Measurements', *J. Fluid Mech.* **162**, 389–413.

Brunet, Y. and Raupach, M. R.: 1987, 'A Simple Renewal Model for Transfer in Plant Canopies', in *Flow and Transport in the Natural Environment: Advances and Application. Poster Abstracts*, International Symposium, Canberra, 31 Aug.–04 Sept. 1987, P4, 2 p.

Collineau, S. and Brunet, Y: 1993, 'Detection of Coherent Motions in a Forest Canopy, Part I: Wavelet Analysis', *Boundary-Layer Meteorol.* **65**, 357–379.

Finnigan, J. J.: 1979, 'Turbulence in Waving Wheat, II. Structure of Momentum Transfer', *Boundary-Layer Meteorol.* **16**, 213–236

Gao, W., Shaw, R. H., and Paw U, K. T.: 1989, 'Observation of Organized Structure in Turbulent Flow within and above a Forest Canopy', *Boundary-Layer Meteorol.* **47**, 349–377.

Paw U, K. T., Brunet, Y., Collineau, S., Shaw, R. H., Maitani, T., Qiu, J., and Hipps, L.: 1992, 'Evidence of Turbulent Coherent Structures in and above Agricultural Plant Canopies', *Agric. For. Meteorol.* **61**, 55–68.

Phong-Anant, D., Antonia, R. A., Chambers, A. J., and Rajalopalan, S.: 1980, 'Features of the Organized Motions in the Atmospheric Surface Layer', *J. Geophys. Res.* **85**, 424–432.

Rajalopalan, S. and Antonia, R. A.: 1982. 'Use of a Quadrant Analysis Technique to Identify Coherent Structures in a Turbulent Boundary Layer', *Phys. Fluids.* **25**, 949–956.

Raupach, M. R., Finnigan, J. J., and Brunet, Y.: 1989, 'Coherent Eddies in Vegetation Canopies', Proc. Fourth Austral. Conf. Heat & Mass Transfer, Christchurch, N-Z, 9–12 May 1989, 75–90.

Schols, J. L. J.: 1984, 'The Detection and Measurement of Turbulent Structures in the Atmospheric Surface Layer', *Boundary-Layer Meteorol.* **29**, 39–58.

Shaw, R. H., Tavangar, J., and Ward, D. P.: 1983, 'Structure of the Reynolds Stress in a Canopy Layer', *J. Clim. Appl. Meteorol.* **22**, 1922–1931.

Shaw, R. H., Paw U, K. T., and Gao, W.: 1989, 'Detection of Temperature Ramps and Flow Structures at a Deciduous Forest Site', *Agr. For. Meteorol.* **47**, 123–138.

Shaw, R. H. and Zhang, X. J.: 1992, 'Evidence of Pressure-Forced Turbulent Flow in a Forest', *Boundary-Layer Meteorol.* **58**, 273–288.

Subramanian, C. S., Rajalopalan, S., Antonia, R. A., and Chambers, A. J.: 1982, 'Comparison of Conditional Sampling and Averaging Techniques in a Turbulent Boundary Layer', *J. Fluid Mech.* **123**, 335–362.